

Simulation design of normally-off AlGaN/GaN high-electron-mobility transistors with p-GaN Schottky hybrid gate

Yun-Long He(何云龙), Fang Zhang(张方), Kai Liu(刘凯), Yue-Hua Hong(洪悦华), Xue-Feng Zheng(郑雪峰),Chong Wang(王冲), Xiao-Hua Ma(马晓华), and Yue Hao(郝跃)

Citation: Chin. Phys. B, 2022, 31 (**6**): 068501. DOI: 10.1088/1674-1056/ac3739
Journal homepage: http://cpb.iphy.ac.cn; http://iopscience.iop.org/cpb

What follows is a list of articles you may be interested in

Impact of oxygen in electrical properties and hot-carrier stress-induced degradation of GaN high electron mobility transistors

Lixiang Chen(陈丽香), Min Ma(马敏), Jiecheng Cao(曹杰程), Jiawei Sun(孙佳惟), Miaoling Que(阙妙玲), and Yunfei Sun(孙云飞)

Chin. Phys. B, 2021, 30 (**10**): 108502. DOI: 10.1088/1674-1056/ac1efd

Performance analysis of GaN-based high-electron-mobility transistors with postpassivation plasma treatment

Xing-Ye Zhou(周幸叶), Xin Tan(谭鑫), Yuan-Jie Lv(吕元杰), Guo-Dong Gu(顾国栋), Zhi-Rong Zhang(张志荣), Yan-Min Guo(郭艳敏), Zhi-Hong Feng(冯志红), and Shu-Jun Cai(蔡树军)

Chin. Phys. B, 2021, 30 (**2**): 028502. DOI: 10.1088/1674-1056/abb7f6

A 2DEG back-gated graphene/AlGaN deep-ultraviolet photodetector with ultrahigh responsivity

Jinhui Gao(高金辉), Yehao Li(李叶豪), Yuxuan Hu(胡宇轩), Zhitong Wang(王志通), Anqi Hu(胡安琪), and Xia Guo(郭霞)\ccclink

Chin. Phys. B, 2020, 29 (**12**): 128502. DOI: 10.1088/1674-1056/abb3eb

Double superlattice structure for improving the performance of ultraviolet light-emitting diodes

Yan-Li Wang(王燕丽), Pei-Xian Li(李培咸), Sheng-Rui Xu(许晟瑞), Xiao-Wei Zhou(周小伟), Xin-Yu Zhang(张心禹), Si-Yu Jiang(姜思宇), Ru-Xue Huang(黄茹雪), Yang Liu(刘洋), Ya-Li Zi(訾亚丽), Jin-Xing Wu(吴金星), Yue Hao(郝跃)

Chin. Phys. B, 2019, 28 (**3**): 038502. DOI: 10.1088/1674-1056/28/3/038502

Synthesis of thermally stable HfO_xN_y as gate dielectric for AlGaN/GaN heterostructure field-effect transistors

Tong Zhang(张彤), Taofei Pu(蒲涛飞), Tian Xie(谢天), Liuan Li(李柳暗), Yuyu Bu(补钰煜), Xiao Wang(王霄), Jin-Ping Ao(敖金平)

Chin. Phys. B, 2018, 27 (**7**): 078503. DOI: 10.1088/1674-1056/27/7/078503

Simulation design of normally-off AlGaN/GaN high-electron-mobility transistors with p-GaN Schottky hybrid gate

Yun-Long He(何云龙)[†], Fang Zhang(张方), Kai Liu(刘凯), Yue-Hua Hong(洪悦华), Xue-Feng Zheng(郑雪峰), Chong Wang(王冲), Xiao-Hua Ma(马晓华), and Yue Hao(郝跃)

Key Laboratory of Wide Band Gap Semiconductor Materials and Devices, School of Microelectronics, Xidian University, Xi'an 710071, *China*

(Received 26 August 2021; revised manuscript received 22 October 2021; accepted manuscript online 6 November 2021)

A novel normally-off AlGaN/GaN high-electron-mobility transistor (HEMT) with a p-GaN Schottky hybrid gate (PSHG) is proposed, and compared with the conventional p-GaN normally-off AlGaN/GaN HEMTs. This structure can be realized by selective etching of p-GaN layer, which enables the Schottky junction and PN junction to control the channel charge at the same time. The direct current (DC) and switching characteristics of the PSHG HEMTs are simulated by Slivaco TCAD, and the p-GaN HEMTs and conventional normally-on HEMTs are also simulated for comparison. The simulation results show that the PSHG HEMTs have a higher current density and a lower on-resistance than p-GaN HEMTs, which is more obvious with the decrease of p-GaN ratios of the PSHG HEMTs. The breakdown voltage and threshold voltage of the PSHG HEMTs are very close to those of the p-GaN HEMTs. In addition, the PSHG HEMTs have a higher switching speed than the conventional normally-on HEMTs, and the p-GaN layer ratio has no obvious effect on the switching speed.

Keywords: normally-off high-electron-mobility transistor, AlGaN/GaN, p-GaN

PACS: 85.30.De, 85.30.Tv **DOI:** 10.1088/1674-1056/ac3739

1. Introduction

AlGaN/GaN-based HEMTs play an increasingly important role in the field of microwave power due to its high breakdown voltage, high electron concentration and high electron mobility.[1–3] Conventional AlGaN/GaN HEMTs are normally-on devices and perform well in the low-voltage and high frequency applications. However, normally-off devices are required to guarantee a safe operation and a simple gate drive configuration in power switching applications. In order to realize the normally-off devices, researchers have adopted many methods, such as fluorine plasma treatment,[4] recessed gate metal insulator semiconductor (MIS),[5] nano channel,[6] and p-GaN cap layer.[7] Among these methods, the devices with p-GaN cap layer are widely used in power supply, wireless charging and other fields, due to its stable threshold voltage and high repeatability of fabrication process.[8–10] However, compared with other normally-off devices, the p-GaN HEMTs have lower current density, lower peak transconductance and weaker gate control ability. Hu *et al.* achieved normally-off HEMT by inserting p-type GaN layer between gate and barrier layer through selective growth method, but the threshold voltage was less than +1 V and the on-state saturation current was only 40 mA/mm.[11] Chiu *et al.* used AlN etch stop layer and a novel digital etch procedure in the epitaxial layer design to obtain a p-GaN normally-off device with a threshold voltage of +1.7 V and on-state saturation current of 280 mA/mm, but it has a high on-resistance of 16.1 Ω·mm.[12] Uemoto and others have grown p-AlGaN layer on AlGaN barrier layer. By etching the p-AlGaN layer between gate source and gate drain, the threshold voltage of the device is up to +1 V, and the saturation output current density is about 200 mA/mm.[13] It can be seen that the current density of p-GaN HEMTs is much lower than that of other normally-off devices.

In this paper, based on p-GaN normally-off AlGaN/GaN HEMTs, we propose a novel normally-off AlGaN/GaN HEMT which features in p-GaN Schottky hybrid gate (PSHG) with a simple fabrication process. The DC characteristics, the breakdown characteristics and the switching characteristics of PSHG HEMTs are simulated by Slivaco TCAD, and compared with the p-GaN HEMTs and conventional HMETs, respectively.

2. Device structure and simulation models

The device structures of the p-GaN HEMTs and the PSHG HEMTs are shown in Figs. 1(a) and 1(b), respectively. The epitaxial structure consists of a 60 nm-thick p-GaN cap layer, a 20 nm-thick AlGaN barrier layer with a 15% Al content, and a 2 μm-thick GaN buffer layer. The gate length, gate-to-source distance and gate-to-drain distance of the device are 1 μm, 0.5 μm and 7 μm, respectively. The fabricating process of PSHG HEMTs is so simple that it does not need to add new process steps. When the p-GaN layer between the gate source and the gate drain is etched, the p-GaN layer below the gate can be selectively etched. Then the gate metal is deposited, so that some gate metals are in direct contact with the AlGaN

[†]Corresponding author. E-mail: ylhe@xidian.edu.cn

© 2022 Chinese Physical Society and IOP Publishing Ltd

layer to form Schottky junction. In this way, both the PN junction and Schottky junction control the channel electrons.

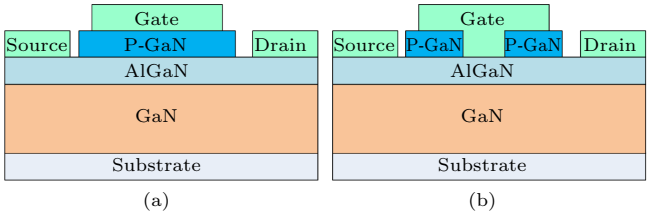


Fig. 1. Schematic device structures of the (a) p-GaN HEMTs and (b) PSHG HEMTs.

The simulations are carried out by using Silvaco TCAD software. Figure 2 shows the structures of the p-GaN HEMTs, the PSHG HEMTs and the conventional normally-on HEMTs. Among these structures, the p-GaN layer ratios of two PSHG HEMTs are 80% and 20%, respectively, as shown in Figs. 2(b) and 2(c). The p-GaN HEMTs and the conventional HEMTs without the p-GaN layer are shown in Figs. 2(a) and 2(d). The hole concentration and mobility of the p-GaN layer are set to be 1×10^{18} cm^{-3} and 10 cm^2/V·s.

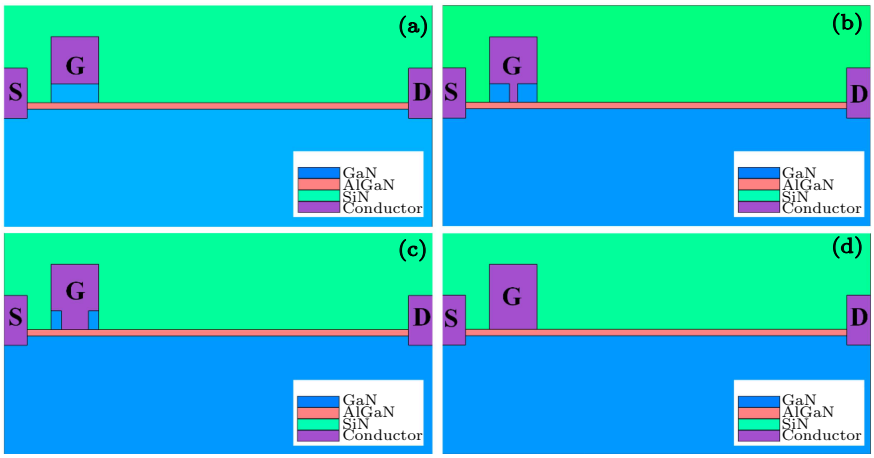


Fig. 2. Simulation device models of (a) p-GaN HEMTs, (b) 80% PSHG HEMTs, (c) 20% PSHG HEMTs and (d) conventional HEMTs.

In the simulation here, the Auger model, the concentration dependent Shockley–Read–Hall model, the parallel electric field dependence model, the polarization model and the Selberherr's impact ionization model are used. Throughout the simulation, a fixed temperature of $T = 300$ K was assumed because the self-heating effect was not a matter of concern in the work. Meanwhile, the contact between gate metal and p-GaN and the contact between the gate metal and p-GaN sidewall are defined as ohmic contacts. The simulation results of p-GaN HEMTs are compared with the experimental results of the devices with the same structural parameters, as shown in Fig. 3. Furthermore, the focus of this paper is on the proposed novel structure concept of PSHG HEMTs based on the conventional p-GaN HEMT structure. The comparative simulation study and the related physical mechanism between the PSHG HEMT and the p-GaN HEMT is sufficiently investigated, which is a big light for the following high current density normally off GaN HEMT fabrication. The model of the PSHG HEMT is established on the basis of the experimentally verified p-GaN HEMT model. Because the p-GaN HEMT inevitably encounters the etching damage, defects and other external problems during the fabrication process. The simulation transfer curve is the same trend but not completely coincident with the actual device transfer curves. However, the experimental results fit well with the simulation results in terms of key device parameters such as threshold voltage, current density, and peak transconductance, which indicates the proposed model of the p-GaN HEMT is accurate. Therefore, the model parameters of p-GaN HEMT can be used for the parameters of the PSHG HEMT model.

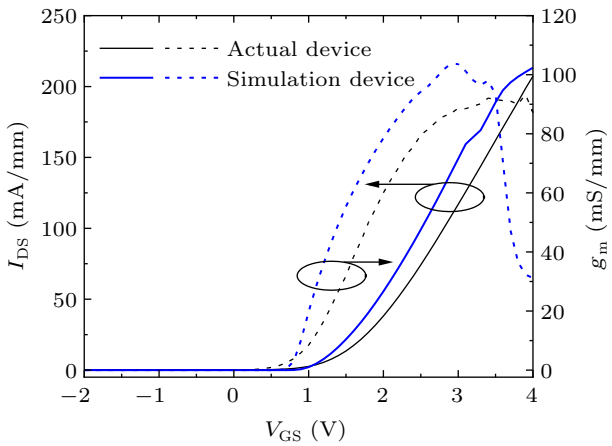


Fig. 3. Comparison of transfer characteristics between simulation device and actual device.

3. Results and discussion

The transfer characteristics of the p-GaN HEMTs, the 80% PSHG HEMTs, the 20% PSHG HEMTs and the conventional normally-on HEMTs at $V_{DS} = 10$ V are shown in Fig. 4(a). It can be seen that the threshold voltage of the p-

GaN HEMTs is the same as that of the PSHG HEMTs with 80% and 20% p-GaN, both of which are +1.0 V. The maximum I_{DS} of the 20% PSHG HEMTs is 315 mA/mm, while that of the p-GaN HEMTs is only 217 mA/mm. The peak transconductance of the p-GaN HEMTs increases from 103 mS/mm to 122 mS/mm of the 20% PSHG HEMTs, which is very close to 130 mS/mm of the conventional normally-on HEMTs without the p-GaN layer. This shows that the p-GaN Schottky hybrid gate can increase the on-state current density and improve the ability of gate to control the channel without changing the V_{TH} when compared with the p-GaN HEMTs. Meanwhile, the smaller the p-GaN layer ratio is, the more obvious the improvement is. Figure 4(b) shows the simulation results of the output characteristics of these four devices at $V_{GS} = V_{TH} + 3$ V, the on-resistance of the p-GaN HEMTs, the 80% PSHG HEMTs, the 20% PSHG HEMTs and the conventional HEMTs are 12.7 Ω·mm, 12.0 Ω·mm, 11.2 Ω·mm and 9.0 Ω·mm, respectively. It shows that the on resistance of the devices can be effectively reduced by decreasing the p-GaN layer ratios. The transfer characteristics curves of four HEMTs under semi-logarithmic coordinates system as shown in Fig. 4(c). It can be seen from the figure that the off-state currents of the four HEMTs are basically maintained at the order of 10^{-10} mA/mm due to the potential etching damage is not considered.

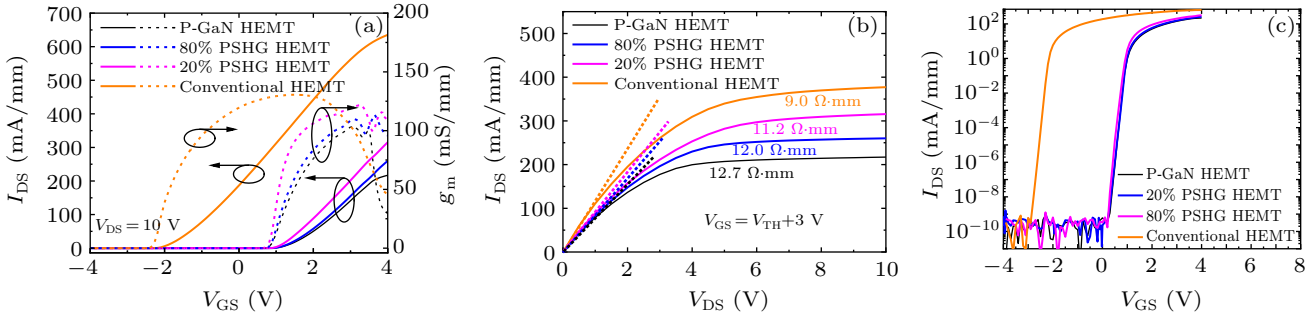


Fig. 4. The DC characteristics of conventional p-GaN HEMTs, 80% PSHG HEMTs, 20% PSHG HEMTs and conventional HEMTs. (a) Transfer curves. (b) Output curves. (c) Transfer curves under semi-logarithmic coordinates system.

The increase of on-state current density by using the p-GaN Schottky hybrid gate probably results from the existence of Schottky barrier, which increases the channel electron concentration. Figures 5(a) and 5(b) show the band diagram of the Schottky junction and the PN junction, respectively.

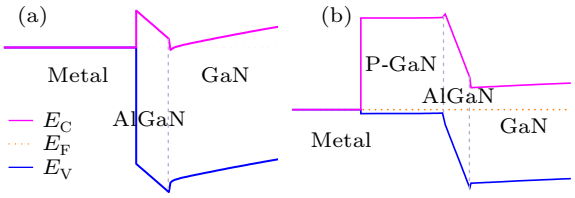


Fig. 5. The band diagram of (a) Schottky junction and (b) PN junction.

Due to the stronger depletion effect of PN junction, the channel electron concentration is lower at the same gate voltage, so the current density of the conventional HEMTs without the p-GaN layer is higher than that of the p-GaN HEMTs. Similarly, due to the existence of both Schottky contact and PN junction, the current density of the PSHG HEMTs is larger than p-GaN HEMTs, and the larger the proportion of p-GaN layer is, the lower the current density is.[14] In addition, due to the existence of Schottky gate, the distance between gate and channel is reduced, which can effectively modulate channel electrons. Therefore, with effective adjustment of the Schottky gate area, the gate control ability is improved, and the peak transconductance increases.[15]

In order to explore the mechanism of the threshold voltage characteristics, the channel electron concentration distribution of the p-GaN HEMTs, the 20% PSHG HEMTs and the conventional HEMTs under zero bias condition were plotted, as shown in the Fig. 6. It can be seen that due to the existence of p-GaN layer, the channel electron concentration below the p-GaN layer is almost depleted, which indicate that the threshold voltage of the PSHG HEMTs seems to have nothing to do with the p-GaN ratio. However, when the p-GaN ratio has been continuously reduced, and the PSHG HEMTs with 16%, 12%, 8%, 4% and 2% of p-GaN ratio are simulated, respectively. The transfer characteristics curves are shown in Fig. 7(a), and the variation curve of threshold voltage with different p-GaN ratio is shown in Fig. 7(b).

It can be seen from the figure that when the p-GaN ratio is lower than 20%, the threshold voltage of the PSHG HEMTs can be negatively shifted, indicating that the depletion effect of the p-GaN layer begins to weaken. Meanwhile, when the p-GaN ratio reaches about 2%, the threshold voltage of PSHG HEMTs is exactly 0, which means that when the p-GaN ratio is less than 2%, p-GaN layer can no longer deplete the channel electrons, and the PSHG HEMTs will become a depletion device.

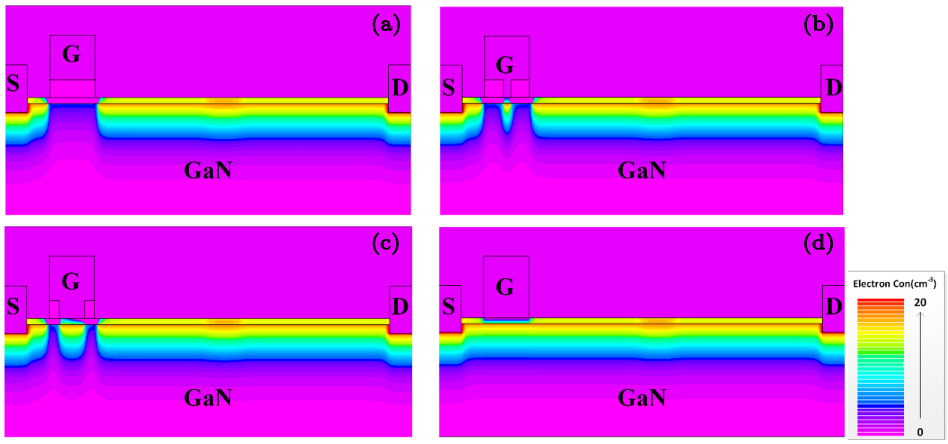


Fig. 6. The channel electron concentration distribution under zero bias condition of (a) p-GaN HEMTs, (b) 20% PSHG HEMTs, (c) 80% PSHG HEMTs, and (d) conventional HEMTs.

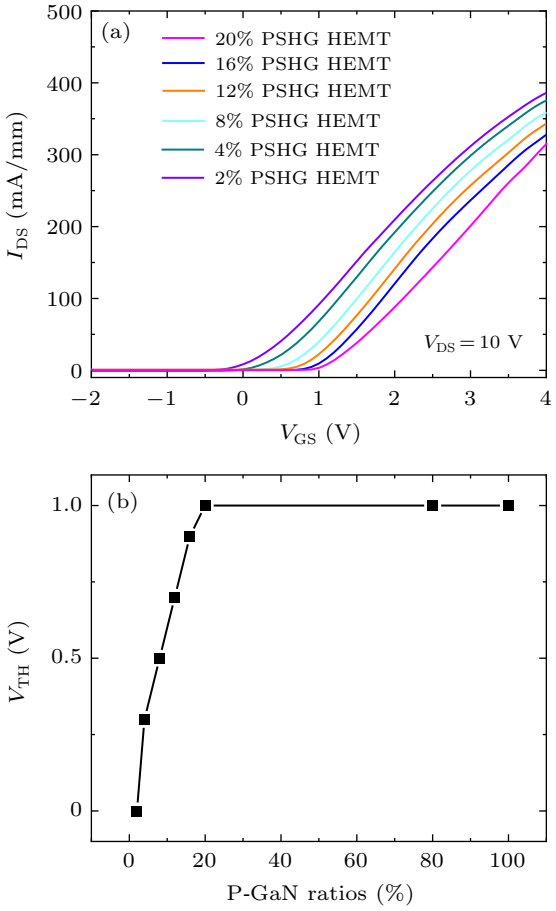


Fig. 7. (a) The transfer characteristics curves of PSHG HEMTs with different p-GaN ratio. (b) The threshold voltage plots as a function of p-GaN ratio.

Figure 8 shows the comparison of the breakdown characteristics of the p-GaN HEMTs, 80% PSHG HEMTs, 20% PSHG HEMTs and the conventional HEMTs. The breakdown voltage of the devices is defined as the drain voltage when drain current is up to 1 μA/mm at $V_{GS} = V_{TH} - 1$ V. The breakdown voltage of the conventional HEMTs is 540 V, while those of the p-GaN HEMTs and the PSHG HEMTs are 620 V. It is obvious that the pGaN layer can improve the breakdown voltage of AlGaN/GaN HEMT, but the reduction of p-GaN layer ratio has little effect on the reverse blocking capability of the device.

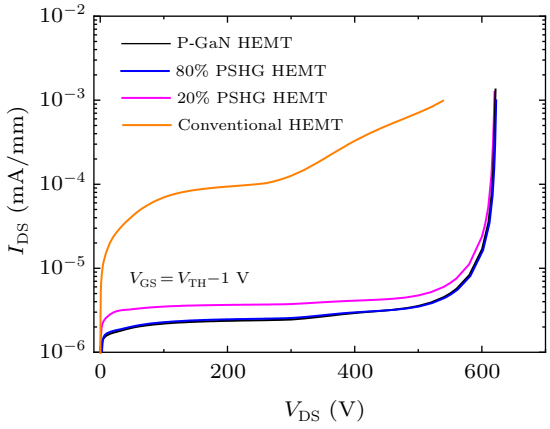


Fig. 8. The breakdown voltage curves of p-GaN HEMTs, 20% PSHG HEMTs, 80% PSHG HEMTs, and conventional HEMTs.

The switching characteristics of the devices are simulated to make a further comparison. The capacitance–voltage (C–V) curves of these four devices are showed in Fig. 9. The three inter-electrode capacitances C_{gs}, C_{gd}, and C_{ds} were simulated, respectively, and then converted into the input capacitance C_{iss} and the output capacitance C_{oss} by using the following equations:[16]

$$C_{iss} = C_{gs} + C_{gd}, \tag{1}$$

$$C_{oss} = C_{gd} + C_{ds}. \tag{2}$$

Here, V_{DS} was set from 0 V to 200 V and all C–V simulations were conducted under $V_{GS} = 0$ V and simulation frequency $f_s = 1$ MHz.[17] As shown in Fig. 9, the gate capacitance of p-GaN HEMTs is lower than that of conventional HEMTs, because the p-GaN HEMTs is a series connection of Schottky barrier capacitance and PN junction capacitance. In addition, it is found that the gate capacitance of p-GaN HEMTs is very close to PSHG HEMTs, indicating that the p-GaN layer ratio can not strongly influence the switching characteristics.

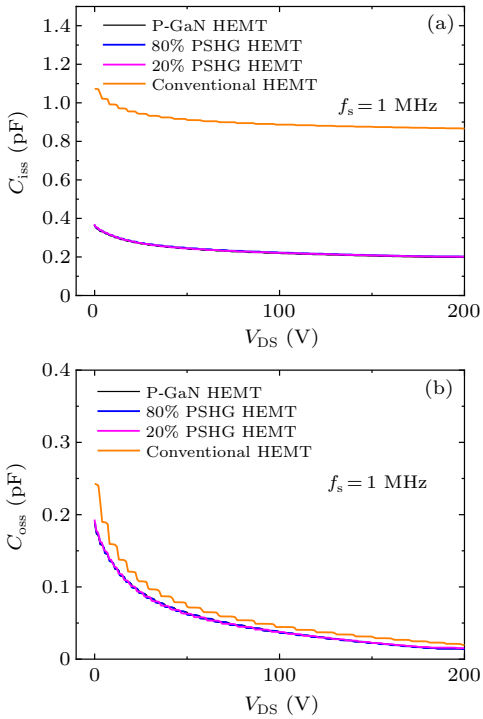


Fig. 9. Simulated *C*–*V* characteristics results of conventional p-GaN HEMTs, 20% PSHG HEMTs, 80% PSHG HEMTs and conventional HEMTs (a) C_{iss} and (b) C_{oss}.

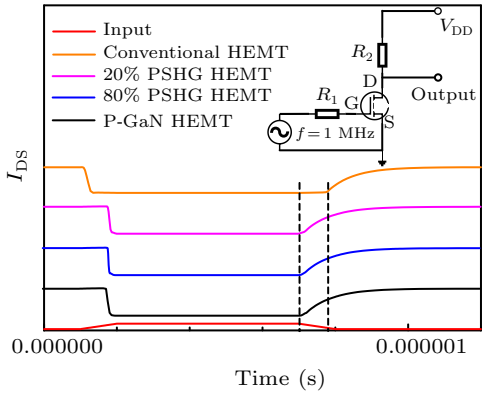


Fig. 10. Simulated switching characteristics results of conventional p-GaN HEMTs, 20% PSHG HEMTs, 80% PSHG HEMTs and conventional HEMTs. The circuit of mix-mode simulation (inset).

In order to show the switching speed of the device more intuitively, mix-mode simulation is used to compare the switching characteristics of the four devices, as shown in Fig. 10. R_1, R_2 and V_{DD} are set to be 100 Ω, 1000 Ω and 10 V in the circuit, respectively. It is obvious that the switching speed of devices with p-GaN layer is faster than that of conventional HEMTs. The p-GaN HEMTs and PSHG HEMTs almost have the same switching speed. These results are consistent with the simulation results of *C*–*V* characteristics.

4. Conclusion and perspectives

As a conclusion, a novel normally-off PSHG HEMT based on p-GaN HEMTs was proposed. Furthermore, the transfer characteristics, output characteristics, breakdown characteristics and switching characteristics of the devices were analyzed in detail by using Slivaco TCAD simulation software. The results show that with the decrease of p-GaN layer ratio, the on-state current density and transconductance of PSHG HEMTs increased, while the on-resistance decreased. The PSHG HEMTs with 20% p-GaN layer ratio show the best characteristics with the current density of 315 mA/mm and the peak transconductance of 122 mS/mm, respectively, which were 45% and 18% larger than that of the p-GaN HEMTs, respectively. In addition, the on resistance of PSHG HEMTs with 20% p-GaN layer ratio was reduced by 1.5 mΩ·mm compared with p-GaN HEMTs, showing better forward characteristics. The threshold voltage and breakdown voltage of PSHG HEMTs with different p-GaN ratios were 1.0 V and 620 V, respectively, which are close to p-GaN HEMTs. In addition, PSHG HEMTs have higher switching speed than conventional normally-on HEMTs, and the p-GaN layer ratio had little effect on the switching speed of PSHG HEMTs.

Acknowledgments

This work was supported by the National Natural Science Foundation of China (Grant No. 62004150), Postdoctoral Science Foundation of China (Grant No. 2018M643575), the Fundamental Research Funds for the Central Universities, and the Innovation Fund of Xidian University (Grant No. JB211104).

References

[1] Jiang Q M, Tang Z K, Liu C, Lu Y Y and Chen K J 2014 *IEEE Trans. Electron Devices* **61** 762
[2] Bo S, Sensale-Rodriguez B, Wang R, Ketterson A and Xing H G 2012 *Proceedings of the 70th Device Research Conference (DRC)*, p. 1
[3] Wang R N, Cai Y and Chen K J 2009 *Solid-State Electron* **53** 1
[4] Cai Y, Zhou Y, Lau K M and Chen K J 2006 *IEEE Trans. Electron Devices* **53** 2207
[5] Singisetti U, Wong M H, Dasgupta S, Nidhi, Swenson B, Thibeault B J, Speck J S and Mishra U K 2011 *IEEE Electron Device Lett.* **32** 137
[6] He Y L, Mi M H, Wang C, Zheng X F, Zhang M, Zhang H S, Wu J, Yang L, Zhang P, Ma X H and Hao Y 2017 *IEEE Electron Device Lett.* **38** 1421
[7] Coffie R, Buttari D, Heikman S, Keller S, Chini A, Shen L and Mishra U K 2002 *IEEE Electron Device Lett.* **23** 558
[8] Meng W J, Zhang F H, Dong G D, Wu J P and Li L 2021 *IEEE Trans. Electron Devices* **36** 4287
[9] Xie H L, Liu Z H, Hu W R, Zhong Z, Lee K, Guo Y X and Ng G I 2021 *IEEE Microw. Wirel. Comm.* **31** 141
[10] Sun R Z, Liang Y C, Yeo Y C, Zhao C Z, Chen W J and Zhang B 2020 *IEEE J Em. Sel. Top. P* **8** 4270
[11] Hu X, Simin G, Yang J, Khan M A, Gaska R and Shur M S 2000 *Electron. Lett.* **36** 753
[12] Chiu H C, Chang Y S, Li B H, Wang H C, Kao H L, Chien F T, Hu C W and Xuan R 2018 *IEEE Trans. Electron Devices* **65** 4820
[13] Uemoto Y, Hikita M, Ueno H, Matsuo H, Ishida H, Yanagihara M, Ueda T, Tanaka Ts and Ueda D 2007 *IEEE Trans. Electron Devices* **54** 3393
[14] Greco G, Iucolano F and Roccaforte F 2018 *Mat. Sci. Semicon. Proc.* **78** 96
[15] Kumar V, Kuliev A, Tanaka T, Otoki Y and Adesida I 2003 *Electron. Lett.* **39** 1758
[16] Wang H X, Wei J, Xie R L, Liu C, Tang G F and Chen K J 2017 *IEEE Trans. Power Electron* **32** 5539
[17] Shenai K, Cavallaro C, Musumeci S and Pagano R 2003 *Proc. 38th IAS Annual Meeting on Conference Record of the Industry Applications Conference*, p. 1794